Table of contents

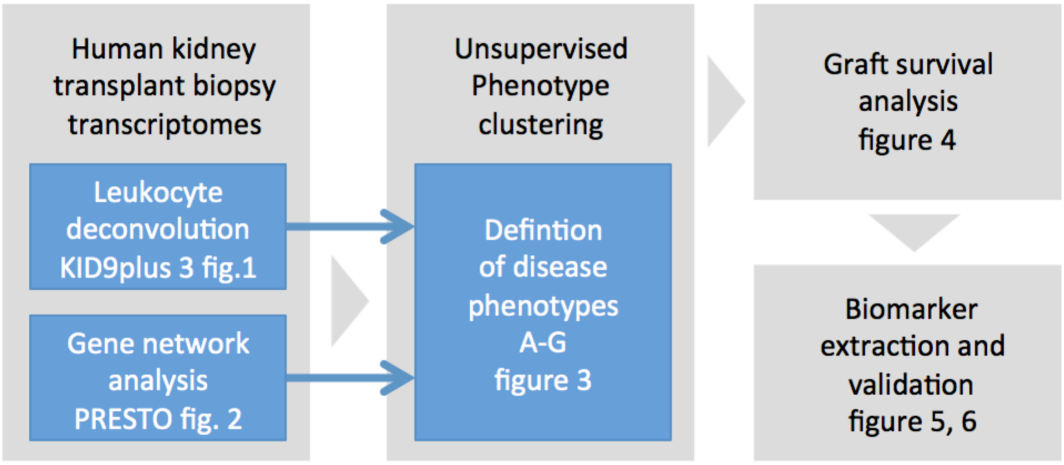

Supplemental figure 1: **Workflow overview.**

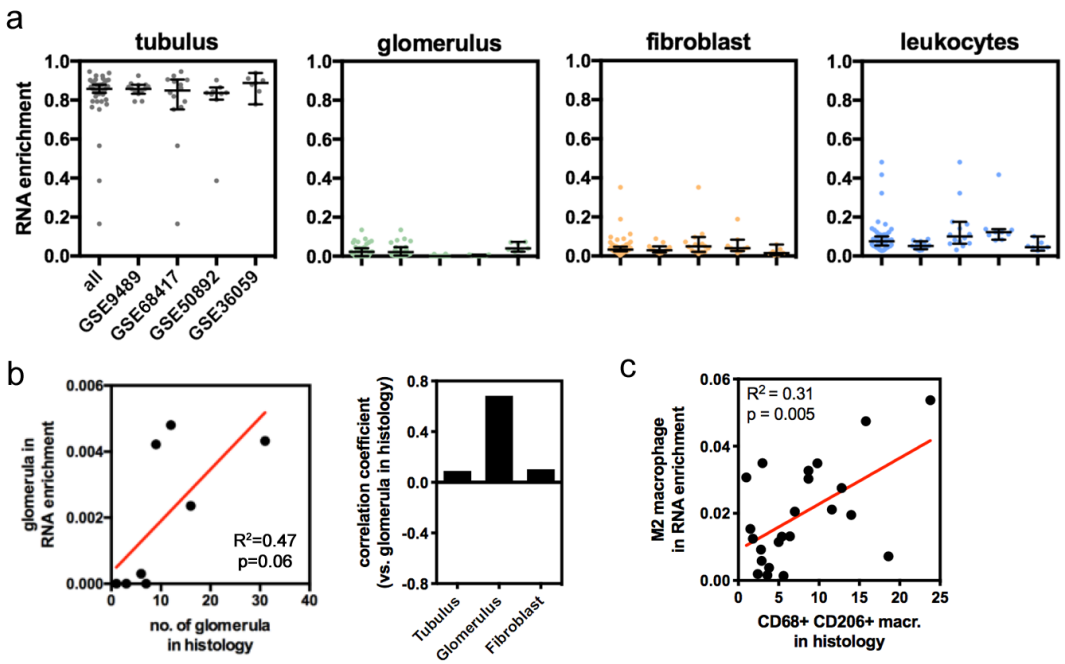

Supplemental figure 2: Validation of leukocyte deconvolution in independent data sets of healthy kidney transplant biopsies. a) The KID9plus3 signature was used to deconvolute GSE36059 (only nephrectomy samples, n=7) and three independent kidney biopsy data sets (GSE9489 n=13, GSE68417 only nephrectomy samples n=14, GSE50892 only normal kidney biopsies n= 9). The enrichment score for tubules, glomeruli, fibroblasts and leukocytes are shown for all data sets. b) The number of glomeruli as counted in histological sections was compared to the glomerulus/tubule/fibroblast enrichment score of KID9plus3 of paired transcriptome samples (GSE50892). c) The KID9plus3 M2 macrophage enrichment score was compared to the number of CD68+ CD206+ macrophages of paired transcriptome samples (GSE65326).

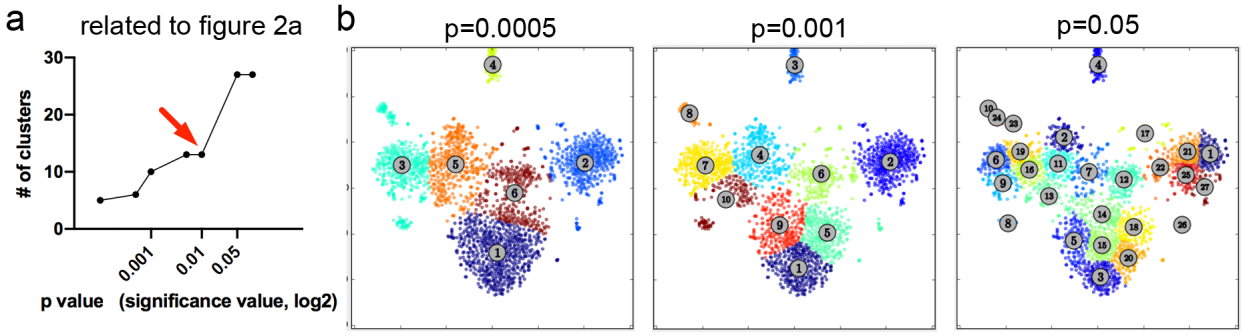

Supplemental figure 3: Cluster sizes depending on user input. a,b) Number of identified PRESTO clusters depending on the significance level in a modified k-means clustering algorithm (see materials and methods). The value of k=0.01 (red arrow) was chosen in manuscript figure 2a.

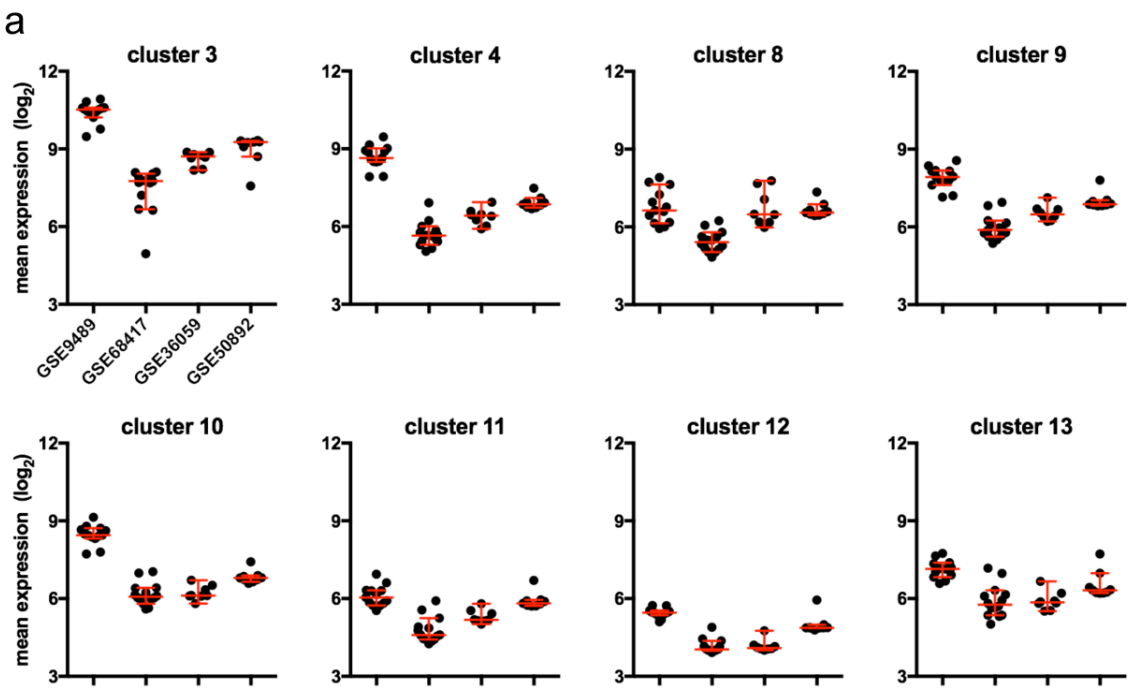

Supplemental figure 4: Gene network analysis in independent data sets of healthy kidney transplant biopsies. Network activity (mean of gene expression per network) for each PRESTO gene network (see main figure 2) was compared across independent data sets. Each dot represents one sample/biopsy. Mean and standard deviation are indicated. (GSE9489 n=13, GSE68417 only nephrectomy samples n=14, GSE50892 only normal kidney biopsies n= 9; see materials and methods).

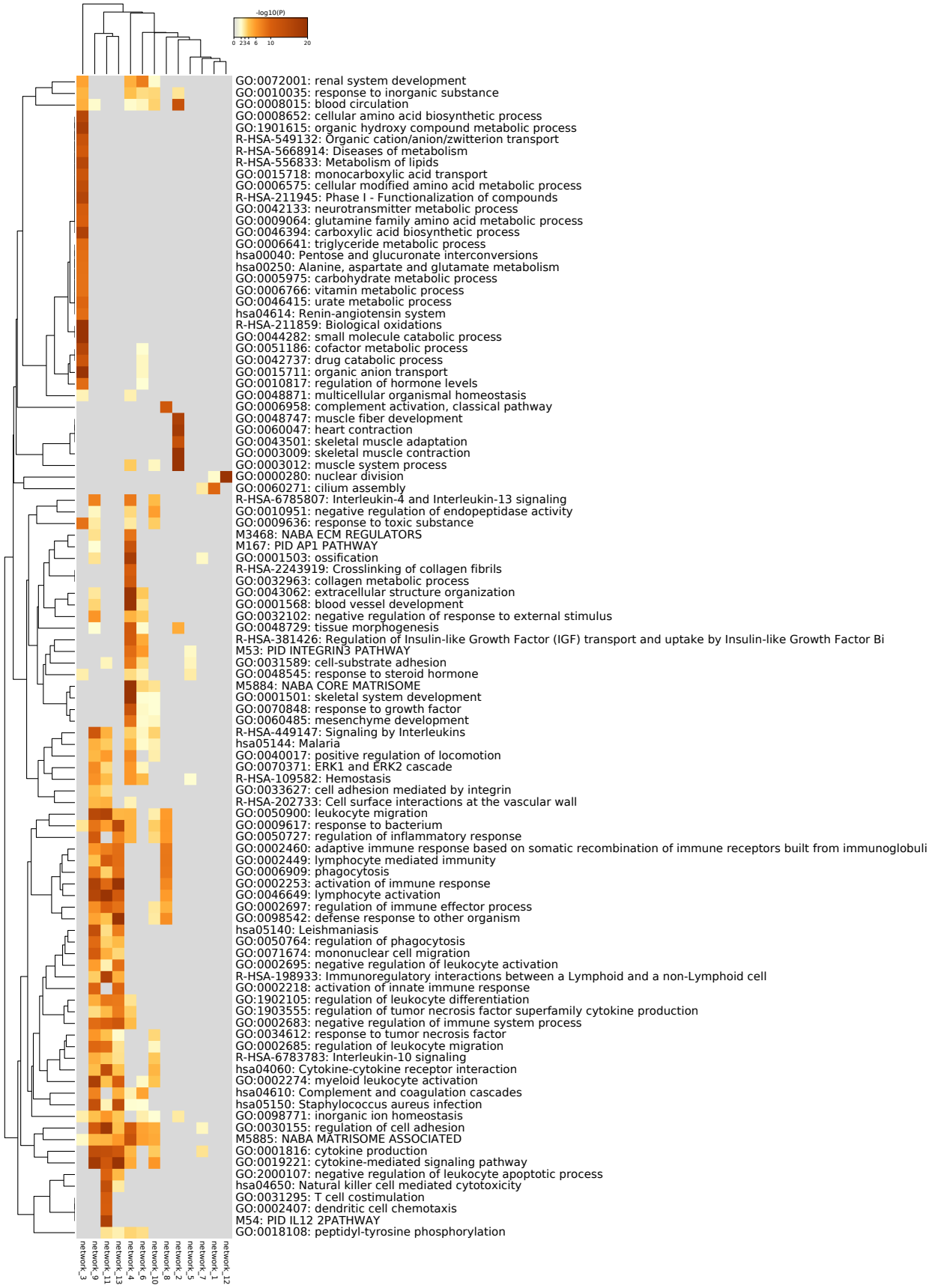
-log10(P)
0 2 3 4 6 10 20
GO:0072001: renal system development
GO:0010035: response to inorganic substance
GO:0008015: blood circulation
GO:0008652: cellular amino acid biosynthetic process
GO:1901615: organic hydroxy compound metabolic process
R-HSA-549132: Organic cation/anion/zwitterion transport
R-HSA-5668914: Diseases of metabolism
R-HSA-556833: Metabolism of lipids
GO:0015718: monocarboxylic acid transport
GO:0006575: cellular modified amino acid metabolic process
R-HSA-211945: Phase I - Functionalization of compounds
GO:0042133: neurotransmitter metabolic process
GO:0009064: glutamine family amino acid metabolic process
GO:0046394: carboxylic acid biosynthetic process
GO:0006641: triglyceride metabolic process
hsa00040: Pentose and glucuronate interconversions
hsa00250: Alanine, aspartate and glutamate metabolism
GO:0005975: carbohydrate metabolic process
GO:0006766: vitamin metabolic process
GO:0046415: urate metabolic process
hsa04614: Renin-angiotensin system
R-HSA-211859: Biological oxidations
GO:0044282: small molecule catabolic process
GO:0051186: cofactor metabolic process
GO:0042737: drug catabolic process
GO:0015711: organic anion transport
GO:0010817: regulation of hormone levels
GO:0048871: multicellular organismal homeostasis
GO:0006958: complement activation, classical pathway
GO:0048747: muscle fiber development
GO:0060047: heart contraction
GO:0043501: skeletal muscle adaptation
GO:0003009: skeletal muscle contraction
GO:0003012: muscle system process
GO:0000280: nuclear division
GO:0060271: cilium assembly
R-HSA-6785807: Interleukin-4 and Interleukin-13 signaling
GO:0010951: negative regulation of endopeptidase activity
GO:0009636: response to toxic substance
M3468: NABA ECM REGULATORS
M167: PID AP1 PATHWAY
GO:0001503: ossification
R-HSA-2243919: Crosslinking of collagen fibrils
GO:0032963: collagen metabolic process
GO:0043062: extracellular structure organization
GO:0001568: blood vessel development
GO:0032102: negative regulation of response to external stimulus
GO:0048729: tissue morphogenesis
R-HSA-381426: Regulation of Insulin-like Growth Factor (IGF) transport and uptake by Insulin-like Growth Factor Bi
M53: PID INTEGRIN3 PATHWAY
GO:0031589: cell-substrate adhesion
GO:0048545: response to steroid hormone
M5884: NABA CORE MATRISOME
GO:0001501: skeletal system development
GO:0070848: response to growth factor
GO:0060485: mesenchyme development
R-HSA-449147: Signaling by Interleukins
hsa05144: Malaria
GO:0040017: positive regulation of locomotion
GO:0070371: ERK1 and ERK2 cascade
R-HSA-109582: Hemostasis
GO:0033627: cell adhesion mediated by integrin
R-HSA-202733: Cell surface interactions at the vascular wall
GO:0050900: leukocyte migration
GO:0009617: response to bacterium
GO:0050727: regulation of inflammatory response
GO:0002460: adaptive immune response based on somatic recombination of immune receptors built from immunoglobuli
GO:0002449: lymphocyte mediated immunity
GO:0006909: phagocytosis
GO:0002253: activation of immune response
GO:0046649: lymphocyte activation
GO:0002697: regulation of immune effector process
GO:0098542: defense response to other organism
hsa05140: Leishmaniasis
GO:0050764: regulation of phagocytosis
GO:0071674: mononuclear cell migration
GO:0002695: negative regulation of leukocyte activation
R-HSA-198933: Immunoregulatory interactions between a Lymphoid and a non-Lymphoid cell
GO:0002218: activation of innate immune response
GO:1902105: regulation of leukocyte differentiation
GO:1903555: regulation of tumor necrosis factor superfamily cytokine production
GO:0002683: negative regulation of immune system process
GO:0034612: response to tumor necrosis factor
GO:0002685: regulation of leukocyte migration
R-HSA-6783783: Interleukin-10 signaling
hsa04060: Cytokine-cytokine receptor interaction
GO:0002274: myeloid leukocyte activation
hsa04610: Complement and coagulation cascades
hsa05150: Staphylococcus aureus infection
GO:0098771: inorganic ion homeostasis
GO:0030155: regulation of cell adhesion
M5885: NABA MATRISOME ASSOCIATED
GO:0001816: cytokine production
GO:0019221: cytokine-mediated signaling pathway
GO:2000107: negative regulation of leukocyte apoptotic process
hsa04650: Natural killer cell mediated cytotoxicity
GO:0031295: T cell costimulation
GO:0002407: dendritic cell chemotaxis
M54: PID IL12 2PATHWAY
GO:0018108: peptidyl-tyrosine phosphorylation
network_3
network_9
network_11
network_13
network_4
network_6
network_10
network_8
network_2
network_5
network_7
network_1
network_12

Supplemental figure 5: Functional annotation of gene networks. Metascape was used to compare significant functional annotations in PRESTO gene networks 1-13 (shown in figure 2). The color codes for the p-value (-log10(p)).

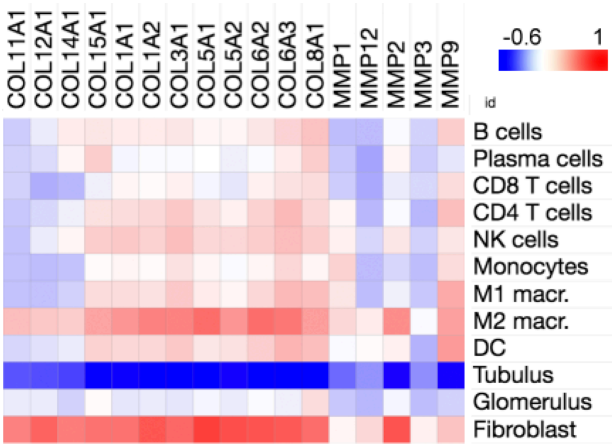

Supplemental figure 6: Collagen and MMP gene correlation with cell types.

Individual genes were Pearson correlated with the KID9plus3 cell type abundance.

GSE36059, n=411.

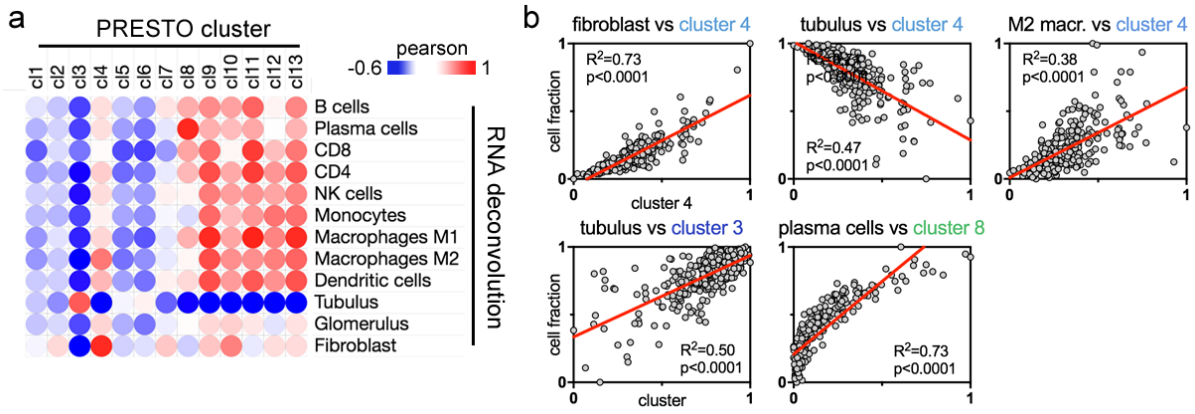

Supplemental figure 7: Cell type specific gene network activity in an independent data set. a) The PRESTO gene network correlation with leukocyte subsets based on RNA deconvolution was performed in an independent data set (GSE21374, n = 282 biopsies) similar to main figure 2d. b) Specific correlations are shown as XY histogram with linear regression analysis.

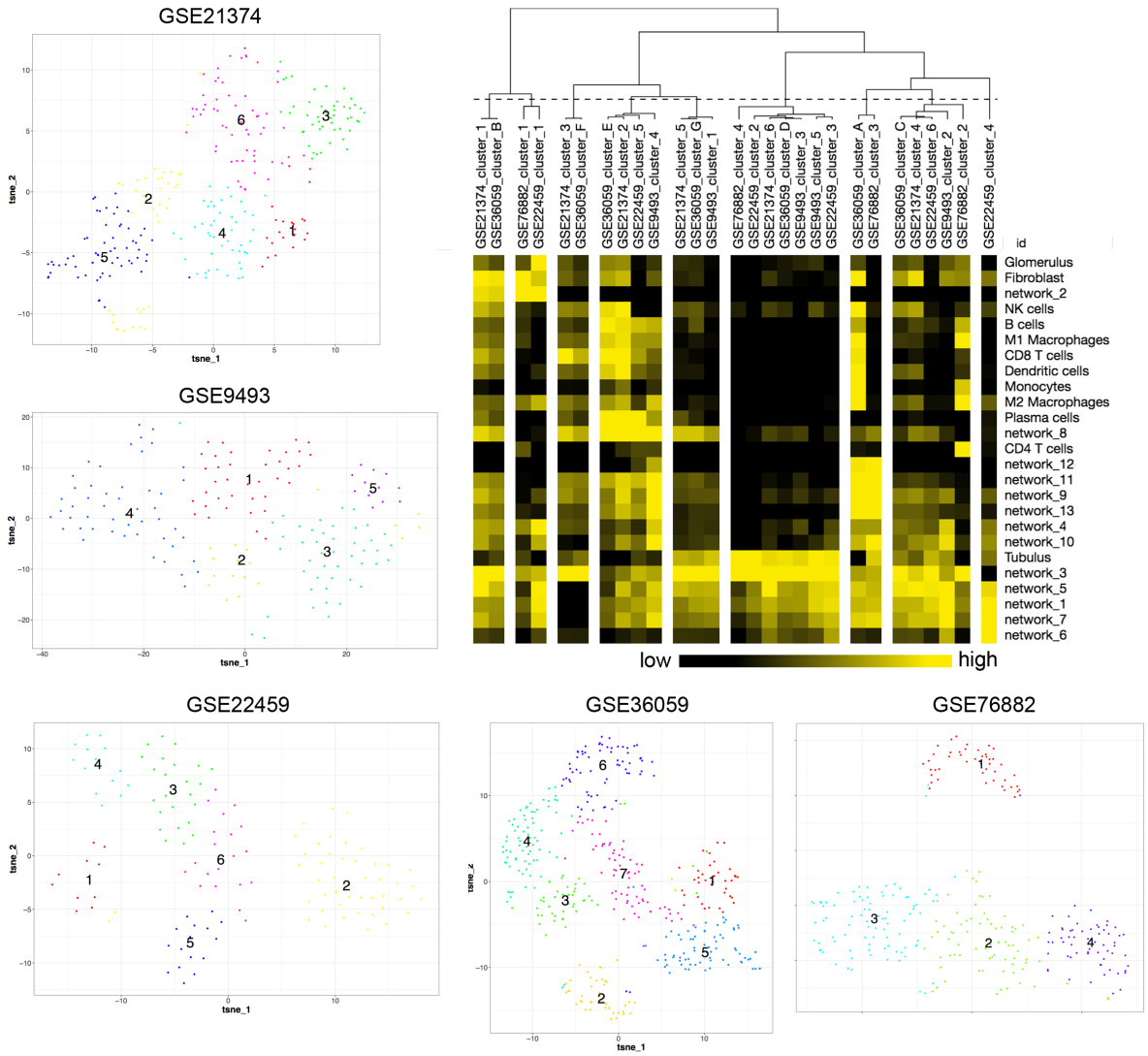

Supplemental figure 8: Immune phenotype clustering in independent data sets. Data driven high dimensional clustering and visualization was performed similar to main figure 3 using independent data sets GSE21374 (n=282), GSE9493 (n=82), GSE22459 (n=65), GSE78662 (n=274) (see materials and methods for more information and the data sets). GSE36059 is also shown in main figure 3. The heatmap shows differential expression patterns of input parameters (PRESTO gene network activity and KID9plus3 leukocyte enumeration). The dendrogram shows hierarchical clustering using Euclidean distance metrics (similar to main figure 3d).

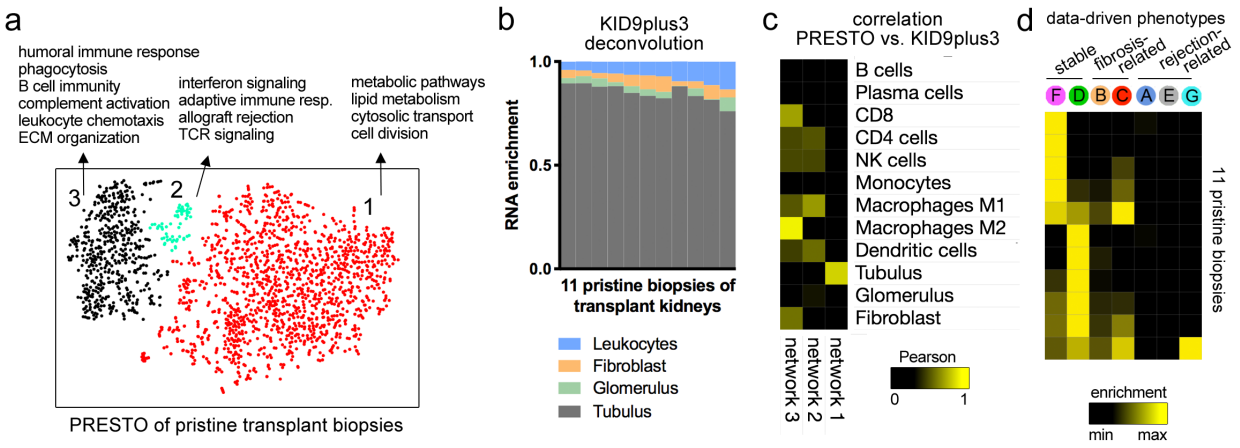

Supplemental figure 9: Immune phenotypes in pristine biopsies. Unsupervised phenotype analysis of pristine kidney transplant biopsies. 11 pristine biopsies from GSE30718 were analyzed similar to our main analysis in the manuscript. a) PRESTO gene network analysis of 1914 genes was performed similar to main figure 2a and resulted in 3 main networks. Enriched pathways for the three networks are shown. b) KID9plus3 deconvolution analysis of pristine biopsies similar to main figure 1c. c) Correlation of leukocyte enumeration data and gene network activity similar to main figure 2d. d) Deconvolution of phenotypes using the 7 phenotypes A-G developed in main figure 3. Phenotypes F and D are annotated as “stable”, C and B as “fibrosis-related”, and A and E as “rejection-related” according to main figure 3.

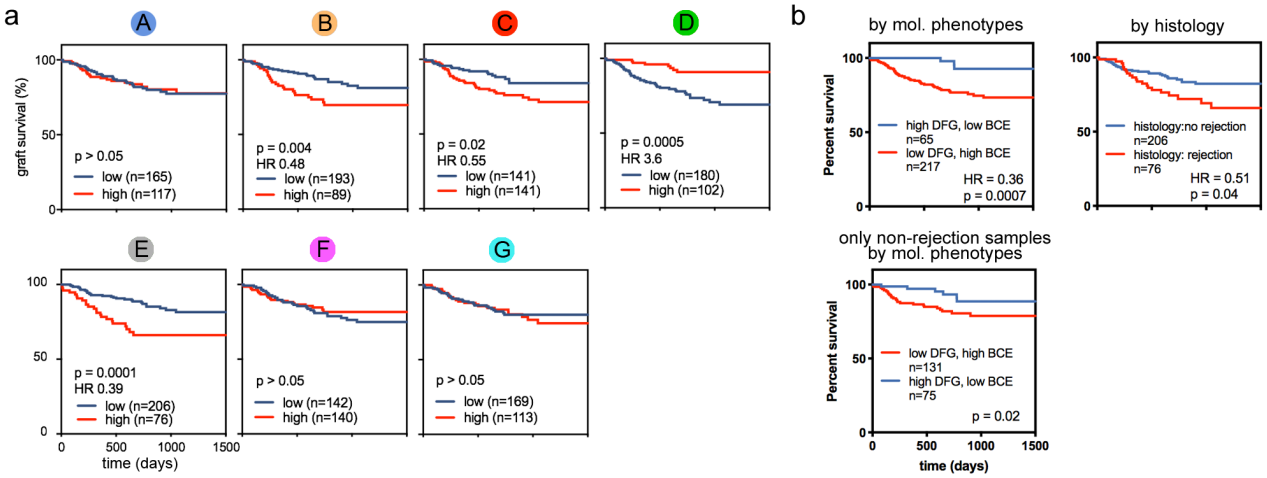

Supplemental figure 10: Graft survival analysis in the independent data set GSE21374. n=282. Related to figure 4. a) The enrichment of each phenotype in each sample was calculated and two groups (high and low expression) were defined based on the enrichment score as described in materials and methods. Hazard ratio (HR) and log rank p-value are indicated. b) Graft survival stratified by histology (rejection versus non-rejection by Banff) versus molecular phenotypes (low survival phenotypes DFG versus high survival phenotypes BCE). The lower panel shows graft survival by molecular phenotypes only in a subcohort of non-rejection biopsies (histology, n=206)

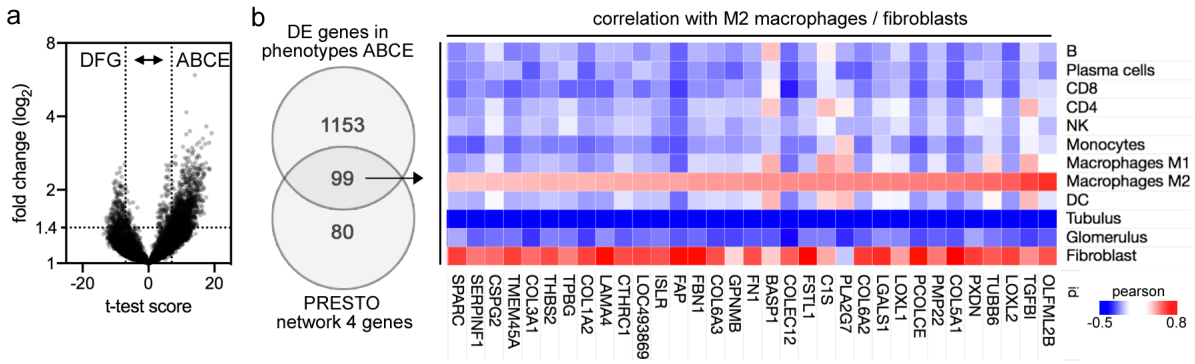

Supplemental figure 11: Molecular candidate markers of dysfunctional transplant phenotypes. a) Differentially expressed genes (DE) were calculated for phenotypes with reduced graft survival (A,B,C,E) versus phenotypes with normal graft survival (D,F,G) (see main figure 3) as described in materials and methods. b) The overlap of DE genes and PRESTO gene network 4 are 99 genes. They were correlated with the calculated cell type abundance and ranked by the KID9plus3 M2 macrophage enrichment score. Highly correlating genes are macrophage/fibroblast-expressed molecular candidates for graft dysfunction.

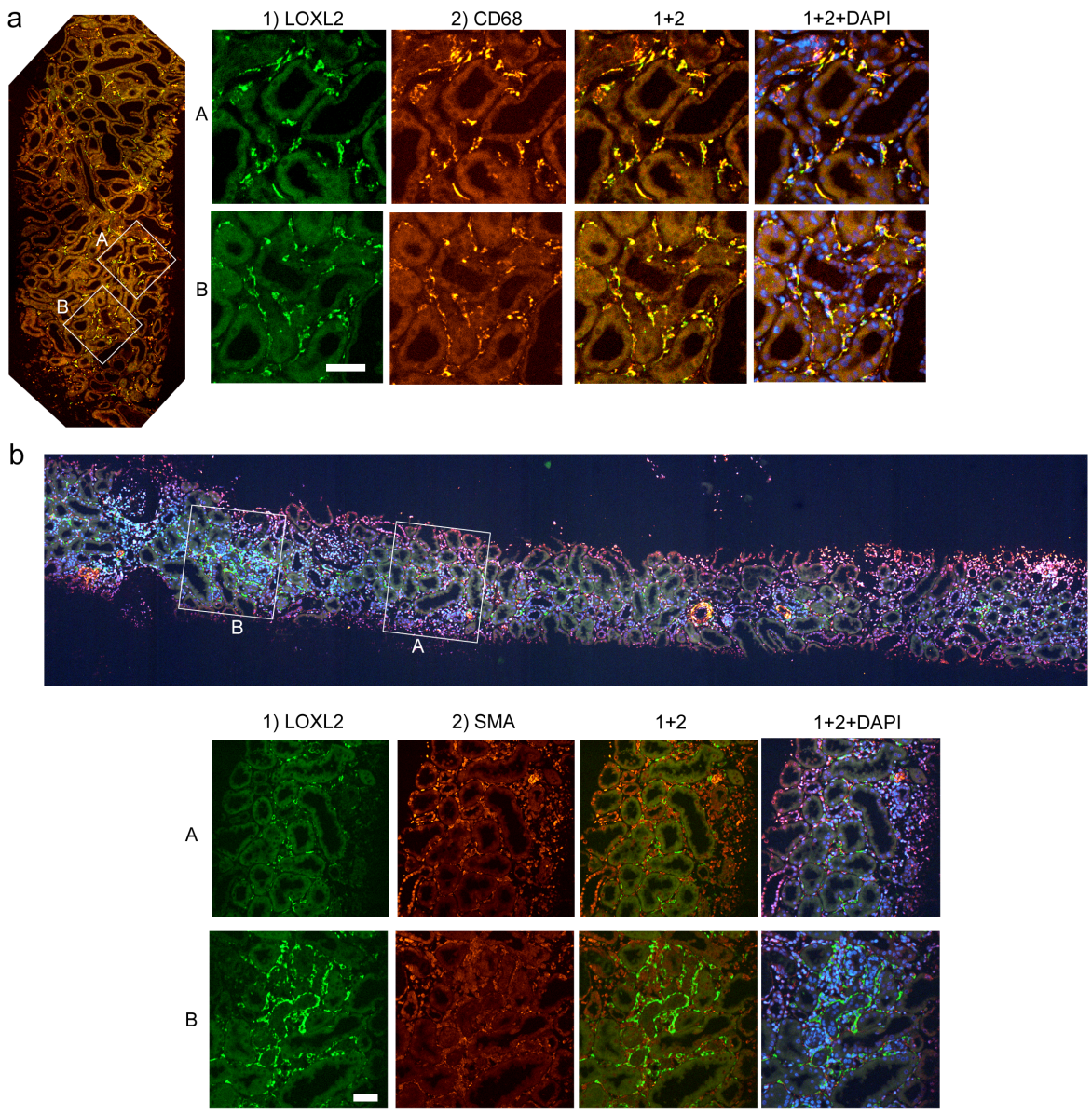

Supplemental figure 12: Immunofluorescence microscopy of LOXL2 in human kidney biopsies. A stitched image of multiple high resolution and multi color confocal micrographs is acquired using clinical kidney transplant biopsies. Nuclear staining with DAPI. Two fields of view are shown in detail. a) LOXL2 and CD68 staining. b) LOXL2 and smooth muscle actin (SMA) staining. Scale bar indicates 100 µm.

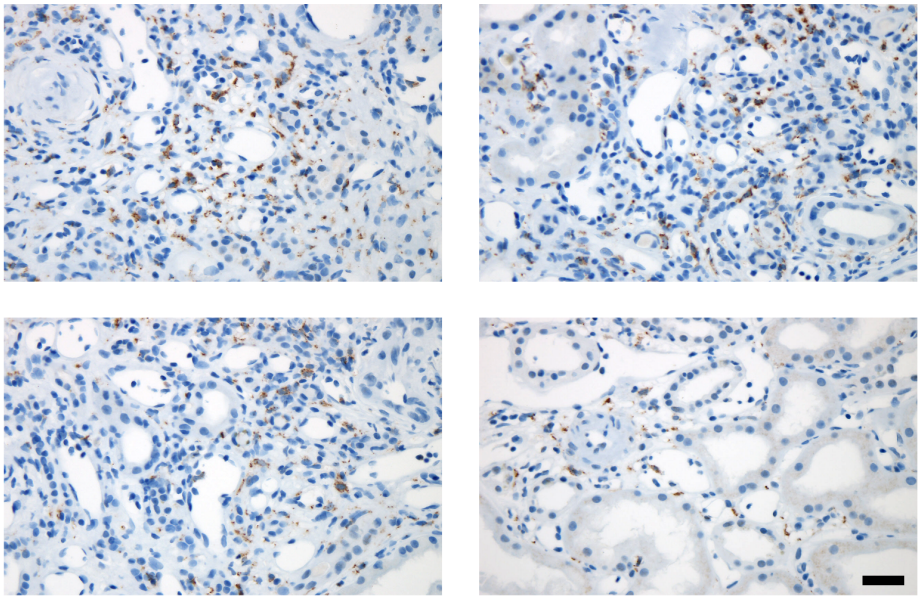

Supplemental figure 13: Immunohistochemical staining of LOXL2 in kidney transplant biopsies. Representative IHC stainings of clinical transplant biopsies are shown. Scale bar 100um.

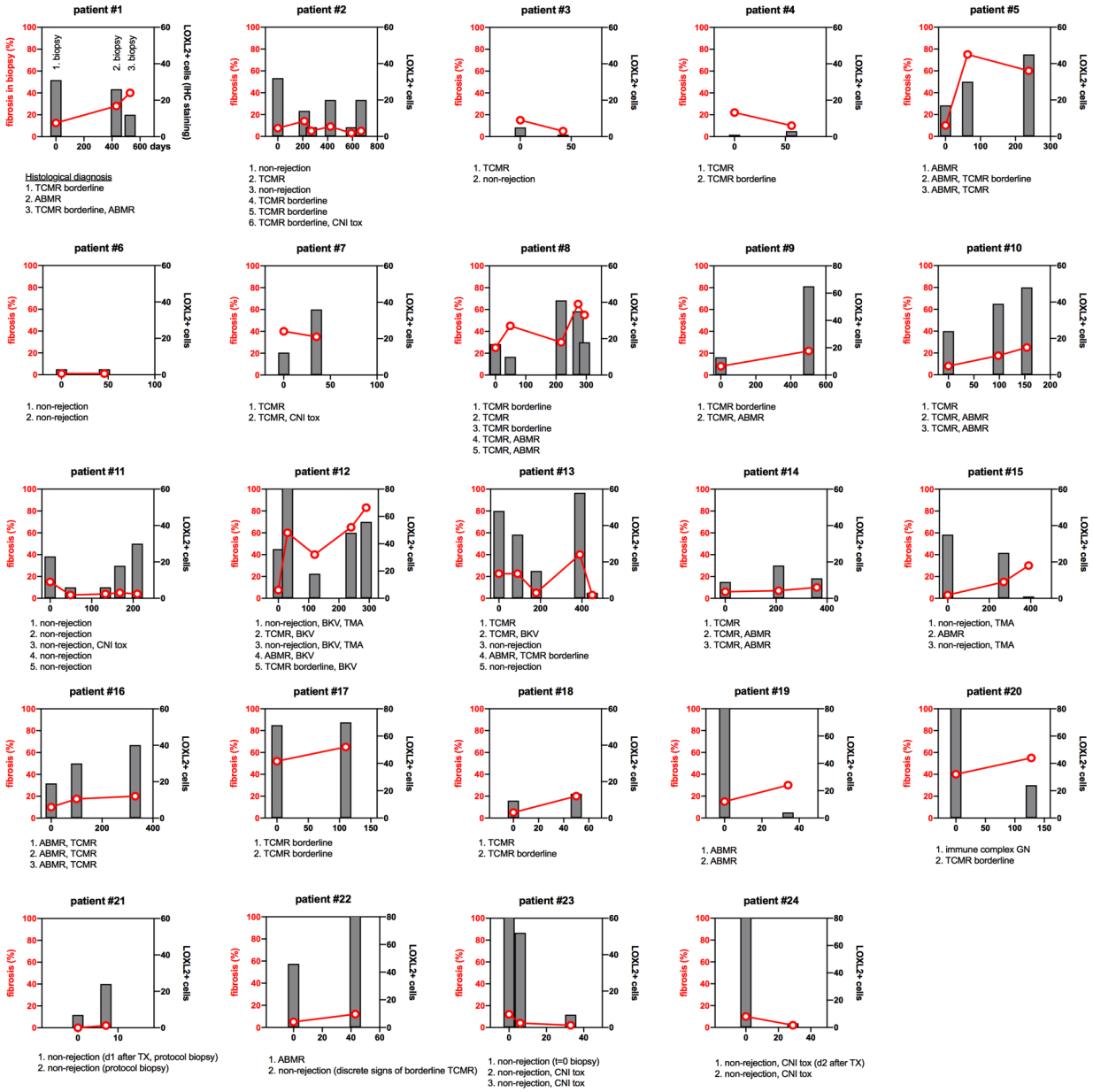

Supplemental figure 14: Quantification of LOXL2+ peritubular macrophages and fibrosis in longitudinal biopsies. 24 kidney transplanted patients were selected that underwent sequential indication biopsies (n=70). For each biopsy the histological fibrosis score (red line) and the LOXL2+ macrophage cell abundance (gray bar) was determined, and the BANFF diagnosis is indicated.

Supplemental table 1: Overview of independent validation data sets.

Supplemental table 2: Gene network composition. For each gene network 1-13 the gene names are indicated.

Supplemental table 3: Functional annotation of gene networks. The functional annotation list of gene networks 1-13 are shown.

Supplemental table 4: Clinical characteristics of the patients studied in figure 6.